Supplementary to "Modelling molecular composition of SOA from toluene photo-oxidation at urban and street scales"

K. Sartelet[1], Z. Wang[1,*], V. Lannuque[1], S. Iyer[3], F. Couvidat[2], T. Sarica[1,**]

May 29, 2024

[1]: CEREA, École des Ponts ParisTech, EDF R&D, IPSL, Marne la Vallée, France
[2]: Institut National de l'Environnement Industriel et des Risques,Verneuil en Halatte, France
[3]: Aerosol Physics Laboratory, Tampere University, FI-33101 Tampere, Finland
*Current address: University of California, Riverside, CA, USA, and National Center for Atmospheric Research, CO, USA
**: Department of Civil and Environmental Engineering, Northeastern University, Boston, MA, USA
Corresponding author: karine.sartelet@enpc.fr

S1. Reduced semi-explicit mechanisms

Three semi-explicit mechanisms were reduced using the GENerator of reduced Organic Aerosol mechanism: the MCM v3.3.1 (Mech. 1), the mechanism from Lannuque et al. (2023) with irreversible methylglyoxal partitioning (Mech. 3). The reduced mechanisms are shown in Fig. 1 and Fig. 2 respectively. Fig. 3 describes the rdc. Mech. 3, which corresponds to the rdc. Mech. 2 with the addition of the ipso-BPR pathway and the formation of methyl benzoquinones. The first oxidation products of the mechanisms are detailed in Table 1, volatile organic compounds in Table 2, and semi and low volatile organic compounds in Table 3 and Table 4 respectively. The reduced mechanisms were evaluated by comparison to the the near-explicit mechanisms over 9431 conditions over Europe, as summarized in Table 1 of the paper. The relative differences between the reduced mechanisms and the near explicit ones are shown at the different spatial locations in Fig. 4.

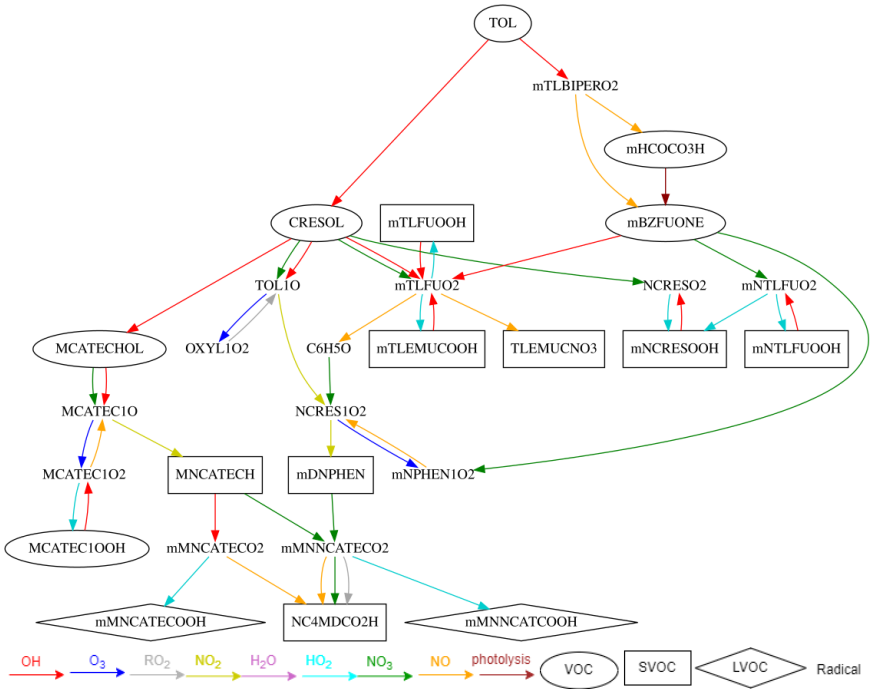

Figure 1: Reduced Mech. 1, corresponding to the reduced mechanism of toluene SOA formation from MCM v3.3.1. SVOC, LVOC corresponds to semi and low-volatility organic compounds of P_{sat} higher and lower than 10^{-9} atm respectively.

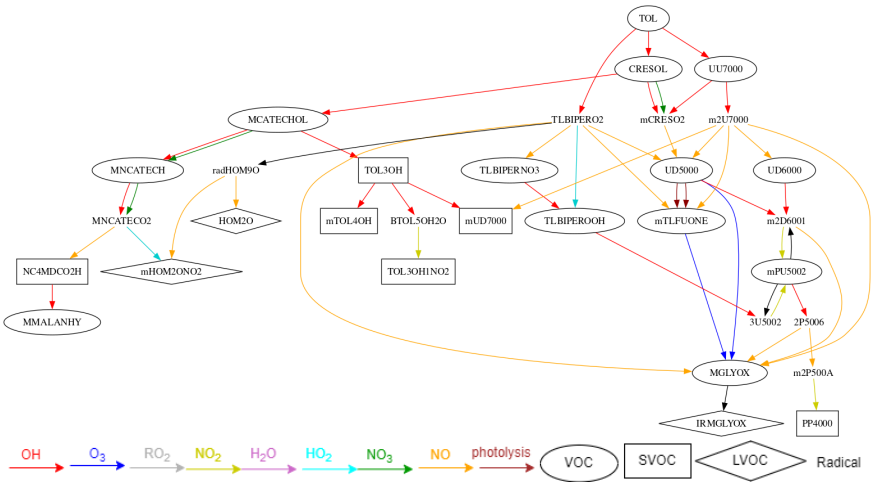

Figure 2: Reduced Mech. 2, corresponding to the reduced mechanism of toluene SOA formation from Lannuque et al. (2023) with irreversible methylglyoxal partitioning.

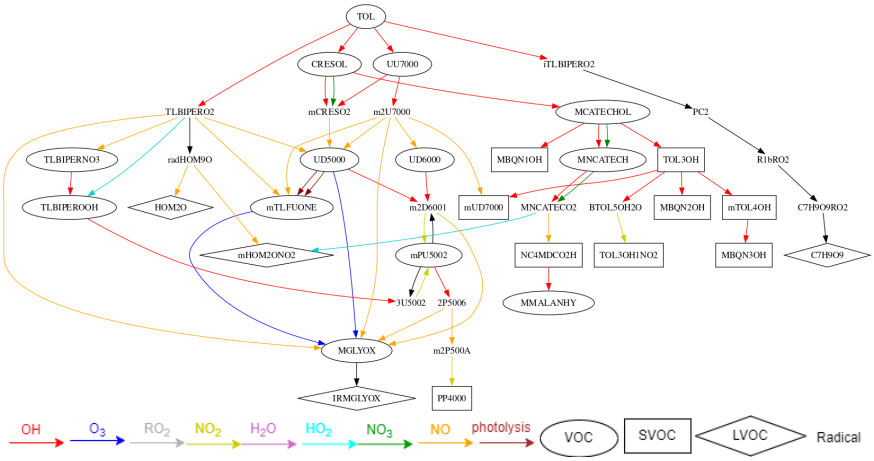

Figure 3: Reduced Mech. 3, corresponding to the Rdc. Mech. 2 with the addition of the ipso-BPR (iTLBIPERO2) pathway and the formation of methyl benzoquinone (MBQN1OH, MBQN2OH, MBQN3OH).

S2. Structures of the compounds

TOL	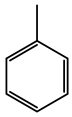	TLBIPERO2	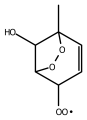
CRESOL	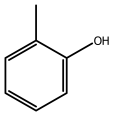	iTLBIPERO2/ipso-BPR	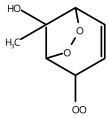
UU7000	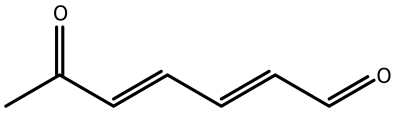		

Table 1: First generation products in the Rdc. Mech. 1, 2 and 3.

MCATECHOL	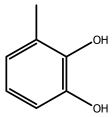	PU5002	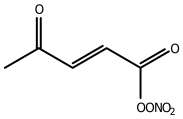
MCATEC1OOH	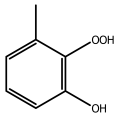	UD5000	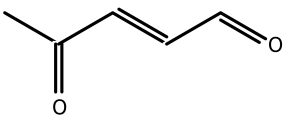
HCOCO3H	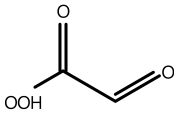	UD6000	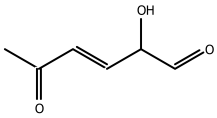
BZFUONE	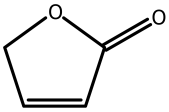	TLBIPERNO3	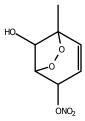
NMALANHY	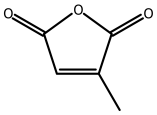	TLBIPEROOH	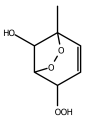
MGLYOX	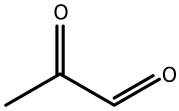		

Table 2: List of volatile organic compounds in Rdc. Mech. 1, 2 and 3.

MNCATECH	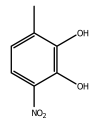	1.53E-04	89.9
MNCATECOOH	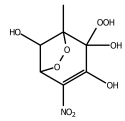	1.70E-11	168
DNPHEN	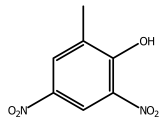	1.49E-04	88.1
NC4MDCO2H	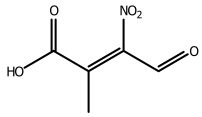	4.04E-05	97.3
MNNCATCOOH	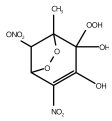	1.13E-11	169
TLEMUCOOH	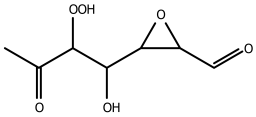	3.16E-07	120
TLEMUCNO3	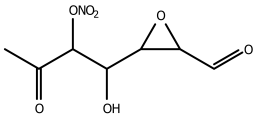	3.20E-06	110
NCRESOOH	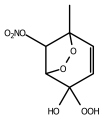	1.39E-06	115
TLFUOOH	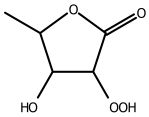	9.34E-06	102
NTLFUOOH	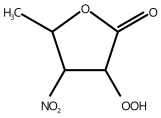	6.67E-06	104

Table 3: List of semi and low volatile organic compounds in Rdc. Mech. 1 with their saturation vapor pressure P_{sat} in torr. at 298 K and enthalpy of vaporisation (ΔH_{vap}).

TOL3OH	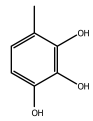	4.53E-05	95.7
TOL4OH	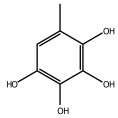	2.50E-07	119
HOM2ONO2	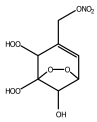	5.63E-11	162
HOM2O	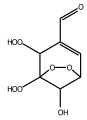	2.73E-09	143
PP4000	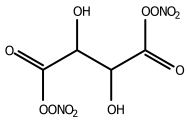	2.66E-06	111
UD7000	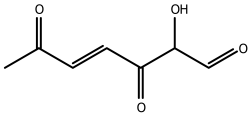	4.18E-05	98.3
TOL3OH1NO2	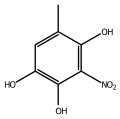	1.07E-06	112
C7H9O9	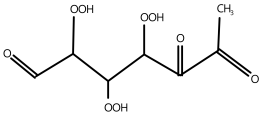 5.9E-13	100	
MBQN1OH	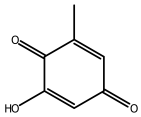	0.003809	77.72
MBQN2OH	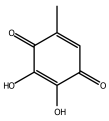 3.025E-5	100	
MBQN3OH	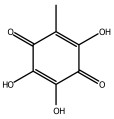	3.025E-7	122.4

Table 4: List of semi and low volatile organic compounds specific to Rdc. Mech. 3 with their saturation vapor pressure P_{sat} in torr. at 298 K and enthalpy of vaporisation (ΔH_{vap}).

S3. Differences between the near-explicit and reduced mechanisms

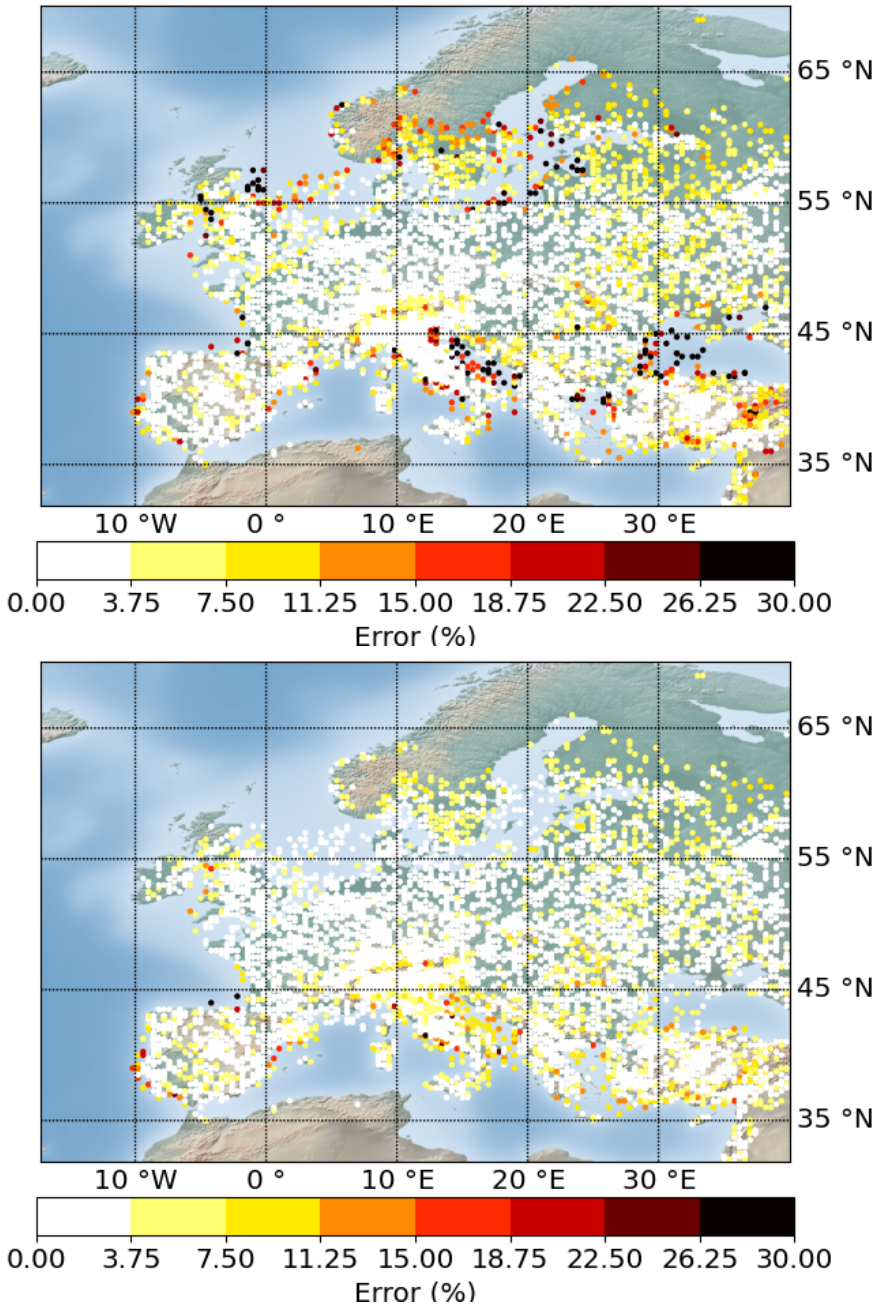

Figure 4: Relative errors between the near-explicit and the reduced mechanisms for Mech. 1 (top panel) and Mech 2 (lower panel) at 9,433 European locations. At each location, three five-day simulations were performed with both the near-explicit and reduced mechanisms for different starting times (0 h, 7 h and 20 h).

S4. Evaluation of the 3D modelling by comparisons to measurements

For the model evaluation, concentrations of regional-scale NO_2, EC, OM, $PM_{2.5}$ and PM_{10} are compared to measurements, using the fractional bias (FB), the geometric mean bias (MG), normalised mean square error (NMSE), geometric variance (VG), normalised absolute difference (NAD), and the fraction of predictions within a factor of 2 of observations (FAC2). Following Hanna and Chang [2012] and Herring and Huq [2018], two different acceptable criteria are considered: (*i*) a strict performance criteria, with $|FB| < 0.3$, $0.7 < MG < 1.3$, $NMSE < 3$, $VG < 1.6$, $NAD < 0.3$, and $FAC2 > 0.5$; and (*ii*) a less strict performance criteria, acceptable for urban areas, with $|FB| < 0.67$, $NMSE < 6$, $NAD < 0.5$, and $FAC2 > 0.5$. As shown in Table 5, the performance criteria for urban areas are met for all pollutants, and the strict performance criteria are met for EC and PM_{10}. The station locations may be viewed in Figure S2 of Sarica *et al.* [2023]. At the street-scale, measurements are performed at one station, and the model to measurement comparison is shown in Table 6. The strict performance criteria are met for for NO_2, $PM_{2.5}$ and PM_{10}.

Table 5: Comparison of regional-scale simulated concentrations and observations in May and June 2014 using rdc. Mech. 3. For each pollutant, the number of stations used in the statistical calculation is specified, followed by the mean measured concentration (Meas. in μg m^{-3}), the mean simulated concentration (Sim. in μg m^{-3}) and the different statistics (FB, MG, NMSE, VG, NAD, FAC2). Note that following Savadkoohi *et al.* [2023], BC concentrations, which are observed with an aethelometer, are normalised by 1.76 to estimate EC concentrations.

	Nb. stats	Meas.	Sim.	FB	MG	NMSE	VG	NAD	FAC2
NO_2	17	20.9	16.5	-0.30	0.71	0.71	2.03	0.29	0.63
$PM_{2.5}$	4	9.9	14.3	0.34	1.43	0.32	1.30	0.20	0.86
PM_{10}	6	17.2	15.8	-0.10	0.90	0.16	1.16	0.15	0.92
EC	1	0.30	0.26	-0.04	0.96	0.14	1.17	0.14	0.96
OM	1	2.5	3.8	0.52	1.75	0.27	1.66	0.23	0.65

Table 6: Comparison of street-scale simulated concentrations and observations in May until 15 June 2014 using rdc. Mech. 3. For each pollutant, the mean measured concentration (Meas. in μg m^{-3}), the mean simulated concentration (Sim. in μg m^{-3}) and the different statistics (FB, MG, NMSE, VG, NAD, FAC2) are specified.

	Meas.	Sim.	FB	MG	NMSE	VG	NAD	FAC2
NO_2	47.4	39.7	-0.19	1.22	0.27	1.26	0.20	0.86
$PM_{2.5}$	12.3	16.9	0.22	0.78	0.46	1.44	0.24	0.75
PM_{10}	20.4	18.5	-0.16	1.18	0.26	1.37	0.20	0.81

S5. Maps of concentrations and concentration differences between the reduced mechanisms

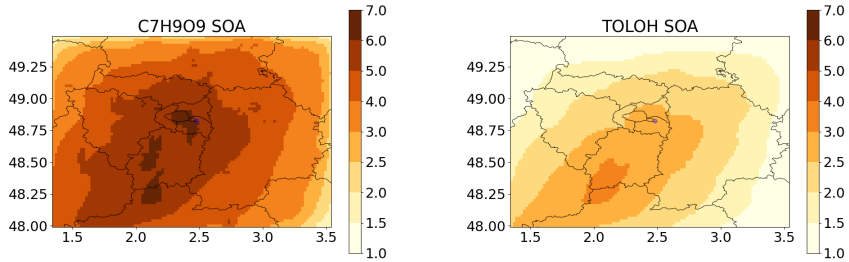

Figure 5: Toluene SOA concentrations simulated in May-June 2014 with Rdc. Mech. 3, from *ipso*-BPR molecular rearrangement (left panel, in ng m^{-3}) and from -OH addition on the aromatic cycle (right panel, in ng m^{-3}).

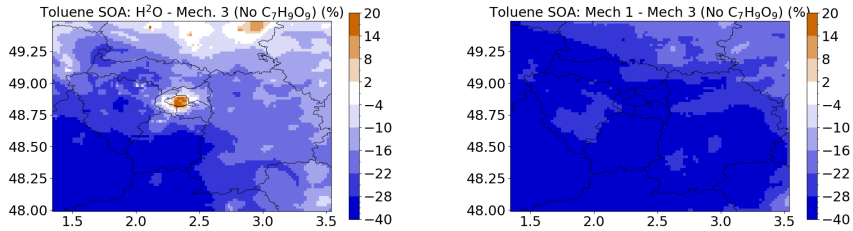

Figure 6: Toluene SOA concentration differences (in %) between H^2O and Rdc. Mech. 2 (left panel) and between Rdc. Mech. 1 and Rdc. Mech. 2 (right panel).

References

S. R. Hanna and J. C. Chang, *Meteorol. Atmos. Phys.*, 2012, **116**, 133–146.

S. Herring and P. Huq, *Fluids*, 2018, **3**, 20.

T. Sarica, K. Sartelet, Y. Roustan, Y. Kim, L. Lugon, B. Marques, B. D'Anna, C. Chaillou and C. Larrie, *Environ. Poll.*, 2023, **332**, 121955.

M. Savadkoohi, M. Pandolfi, C. Reche, J. Niemi, D. Mooibroek, G. Titos, D. Green, A. Tremper, C. Hueglin, E. Liakakou, N. Mihalopoulos,

I. Stavroulas, B. Artiñano, E. Coz, L. Alados-Arboledas, D. Beddows, V. Riffault, J. Brito, S. Bastian, A. Baudic, C. Colombi, F. Costabile, B. Chazeau, N. Marchand, J. Gómez-Amo, V. Estellés, V. Matos, E. Gaag, G. Gille, K. Luoma, H. Manninen, M. Norman, S. Silvergren, J. Petit, J. Putaud, O. Rattigan, H. Timonen, T. Tuch, M. Merkel, K. Weinhold, S. Vratolis, J. Vasilescu, O. Favez, R. Harrison, P. Laj, A. Wiedensohler, P. Hopke, T. Petäjä, A. Alastuey and X. Querol, *Environ. Int.*, 2023, **178**, 108081.